On the Design, Modeling and Control of a Novel Compact Aerial Manipulator

D. Wuthier, D. Kominiak, C. Kanellakis, G. Andrikopoulos, M. Fumagalli, G. Schipper and G. Nikolakopoulos

***Abstract*— The aim of this article is to present a novel four-degree-of-freedom aerial manipulator allowing a multirotor Unmanned Aerial Vehicle (UAV) to physically interact with the environment. The proposed design, named CARMA (*Compact AeRial MAnipulator*), is characterized by low disturbances on the UAV flight dynamics, extended workspace (with regard to its retracted configuration) and fast dynamics (compared to the UAV dynamics). The dynamic model is formulated and a control structure consisting of an inverse kinematics algorithm and independent joint position controllers is presented. Furthermore, the design specifications of the prototype are analyzed in detail, while experimental evaluations are conducted for the extraction of the manipulator's workspace and the evaluation of system's tracking capabilities over pick-and-place trajectories. Finally, it is shown that the selected joint position sensors, combined with the derived inverse dynamic algorithm allow to determine the wrenches exerted at the base, due to swift motions of the arm.**

Fig. 1. The *Compact AeRial MAnipulator* (CARMA) mounted on the ASCTEC NEO platform [8].

I. INTRODUCTION

During the last decade, Unmanned Aerial Vehicles (UAV) have been studied extensively as a way to perform remote sensing, as for example visual inspection tasks, aerial mapping or video recording. Consequently, various configurations have been developed, such as fixed wing and multirotor platforms [1], [2]. Currently, the research in the field is aiming towards the field of aerial interaction with the environment and thus specific focus is addressed in providing UAVs with manipulation capabilities [3].

Up to now, developments towards this vision focused mainly on pick-and-place operations and load transportation. In [4], a quadrotor was equipped with a gripper mounted underneath its base and was used for building simple structures in static environments, while implementing a novel construction algorithm and a corresponding control scheme. Similarly, in [5], an upward directed hand gripper was attached on top of the main body of the aerial vehicle to perform tasks at high altitudes. Moreover, in [6], an aerial payload transportation system was developed by using a main-tail-rotor helicopter with a gripper, while in [7], a cooperative control for payload transportation by multiple quadrotors was proposed in order to achieve specific attitude and position of a payload via the use of cables.

More complicated designs imply a manipulator arm mounted on aerial platforms, towards the vision of co-manipulation and co-interaction with the environment, introducing new disturbances due to variations of Center of Gravity (CoG) and inertial forces. In this area, there has been an increasing interest for designing and controlling such manipulators with the aim to reduce disturbances. In [9], a UAV equipped with two two-Degree-of-Freedom (2-DoF) arms was used for turning a valve by taking into consideration the manipulator-UAV coupling, while in [10], a lightweight and versatile 3-DoF delta manipulator equipped with a 4-DoF end-effector has been secured on a ducted-fan UAV for performing ultrasonic contact inspection. Furthermore, in [11], a hybrid visual servoing control framework for physical interaction using a 6-DoF arm was evaluated, while in [12], a lightweight 5-DoF aerial manipulator was mechanically designed for being compact and minimizing the distance between both arm and UAV CoGs. Finally, in [13], the dynamical coupling between an industrial manipulator and a helicopter type UAV has been addressed by installing a Force/Torque (F/T) sensor at the manipulator-UAV interface and feeding the resulting measurements to the helicopter controller.

In this paper, a novel 4-DoF aerial manipulator design, the *Compact AeRial MAnipulator* (CARMA), that is being mounted underneath a multirotor UAV (see Fig. 1), is

D. Wuthier, D. Kominiak, C Kanellakis, G.ndrikopoulos and G.ikolakopoulos are with the Robotics Group at Division of Systems and Signals, Department of Computer Science, Electrical and Space Engineering, Luleå University of Technology, SE–97187, Luleå, Sweden

M. Fumagalli is with the Vision and Machine Intelligence Lab, Department of Mechanical and Manufacturing Engineering

G. Shipper is with the Saxion University of applied Science, The Netherlands.

This work has received funding from the European Unions Horizon 2020 Research and Innovation Programme under the Grant Agreement No.644128, AEROWORKS

Corresponding Author's email: geonik@ltu.se

©2016 IEEE

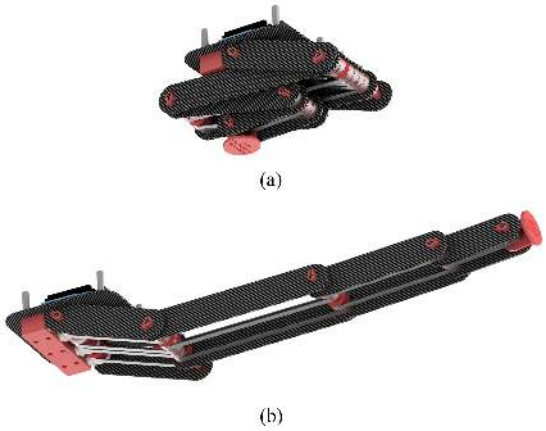

Fig. 2. Visual representation of CARMA in its (a) retracted state and (b) extended state.

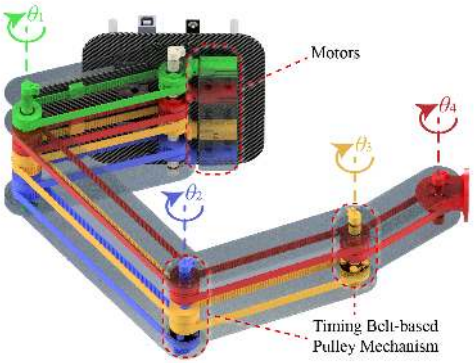

Fig. 3. Conceptual design of the aerial manipulator that highlights the timing-belt pulley mechanisms utilized for the motion of the respective four joints.

proposed for extending the available workspace beyond the perimeter delimited by the propellers. The second contributions of this article stems from the frame design that has been made in such a way to allow the air flow generated by these propellers to circulate through it, thus reducing its drag and thereby the disturbances induced on the flight dynamics. Finally the third contribution is the fact that in order to compensate for the dynamic coupling of the arm on the aerial platform, one requires first the exerted wrenches on the base to be estimated. For the case of inertial, centrifugal and gravitational forces, it has been shown that without requiring any additional sensors, the selected joint position sensors, in combination with a proper inverse dynamic algorithm, can provide relevant data with respect to these wrenches.

The rest of this paper is organized as follows. The conceptual design of the manipulator is described in Section II, while the dynamic model is mathematically formulated and the control architecture are presented in Section III. The hardware and software components, utilized for the development of the prototype, are presented in detail in Section IV. In Section V, the workspace of the manipulator is experimentally acquired, the closed-loop system is evaluated in a pick and place scenario and the dynamical model is experimentally verified. Finally, concluding remarks and discussions about future works are drawn in Section VI.

II. CONCEPTUAL DESIGN

CARMA is intended to provide a multi-rotor UAV, such as the ASCTEC NEO, with capabilities to physically interact with the environment, be it for tasks as pick-and-place operations, load transportation, contact inspections or repairs using dedicated tools. The last link of the manipulator has been designed as a versatile support for various end-effector types. The presented design exhibits the following features:

- Low mass (350 g) and low inertia with respect to the UAV's CoG, thus minimizing the impact on the UAV dynamics.
- Wide workspace, overstepping the propeller blades perimeter, while remaining compact in retracted state (see Fig. 2) and thus allowing not to interfere during take off and landing phases by fitting a 200x130x130 mm envelope.
- Low manufacturing complexity, assuming carbon fiber plate milling and PLA (Polylactic Acid) 3D printing to be available.

The amount of links was set to four in order to achieve long extensions, while keeping a compact retracted state. All four motors are located in the base (Fig. 3), thus rising the manipulator CoG closer to the UAV's CoG, hence minimizing the overall system inertia.

As conceptually depicted in Fig. 3, mechanical power is transmitted from the motors to the joints via bevel gears, in series with timing belt and pulleys mechanism (Fig. 6a). These belts were deliberately not enclosed in order to allow the air flow generated by the propellers to circulate through the frame, thus minimizing the disturbances due to the resulting drag.

When the efforts, exerted on the joints, overcome a certain threshold, the bevel gears act as fuse mechanisms, releasing mechanical stress by hopping gear teeth. Otherwise, the series of gears act as a non-backdrivable mechanisms, allowing the reduction of power consumption, while performing tasks that require the adoption of a static configuration by the arm.

Assignation of motors to joints has been made in such a way to keep the CoG as close as possible to the plane of symmetry of the base. It has to be noted that the link supporting the joint 1 still consists of the base, which is fixed to the UAV. Joint position feedback is achieved by clipping linear potentiometers on the first array of belts (that is to say, the one closest to the base), therefore requiring no zero-initialization, conversely to common incremental encoders.

Another characteristic of CARMA is the fact that the rotation of a single joint will cause only the corresponding link to rotate and translate, while the ones toward the tip only translate and the one toward the base remain steady.

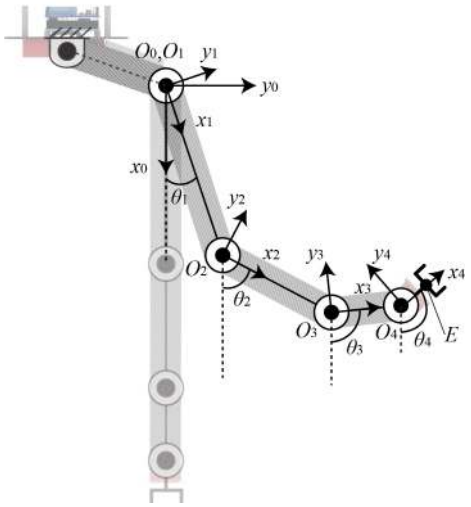

Fig. 4. Schematic representation of CARMA.

III. MODELING AND CONTROL

A. Dynamic Model

The dynamic model presented in this Section is derived by applying a Recursive Newton-Euler Algorithm (RNEA), [14], [15]. According to Fig. 4, the Newton-Euler equations are expressed for each of the links in the base link reference frame (O_0, x_0, y_0, z_0). Simplifications are made as the problem remains planar (no gyroscopic forces, no force along z_0 and moments only along z_0). Such assumptions require the link i, defined as $i = 1,2,3,4$, to have its principal axis of inertia aligned with x_i, y_i and z_i. Thus, only the moment of inertia along z_i remains relevant.

Let F_{ix}, F_{iy} and M_{iz} be vertical/horizontal force components and torques, respectively, applied on link i at O_i. Once the acceleration of each of the links is calculated, the problem is solved recursively for all F_{ix}, F_{iy}, M_{iz} from link 4 to link 1, by assuming no contact force at the end-effector E. Such calculations yield the following results for the forces and torque exerted at the base (written in compact form):

$$\begin{bmatrix} F_x \\ F_y \\ M_z \end{bmatrix} = \boldsymbol{B}(\boldsymbol{q})\ddot{\boldsymbol{q}} + \boldsymbol{C}(\boldsymbol{q},\dot{\boldsymbol{q}})\dot{\boldsymbol{q}} + \boldsymbol{g}(\boldsymbol{q}). \tag{1}$$

$\boldsymbol{q} = \begin{bmatrix} q_1 & \cdots & q_4 \end{bmatrix}^T = \begin{bmatrix} \theta_1 & \cdots & \theta_4 \end{bmatrix}^T$ being the joint coordinates vector and $\boldsymbol{B} : \mathbb{R}^4 \to \mathbb{R}^{3\times4}$, $\boldsymbol{C} : \mathbb{R}^4, \mathbb{R}^4 \to \mathbb{R}^{3\times4}$ and $\boldsymbol{g} : \mathbb{R}^4 \to \mathbb{R}^3$ representing the inertial, centrifugal and gravitational forces, respectively.

In order to apply the proposed model, the following geometrical and inertial parameters have to be defined for link i: a_i, the distance between O_i and O_{i+1}, l_i, the x-coordinate of ith link's CoG (y and z-coordinates are assumed to be zero), its mass m_i and its moment of inertia I_{iz} (along z_i). These parameters were evaluated using the CAD model of CARMA (see table I).

TABLE I

GEOMETRICAL AND INERTIAL PARAMETERS OF THE DYNAMICAL MODEL.

i	l_i [mm]	a_i [mm]	m_i [g]	I_{iz} $\times 10^{-6}$ [kg·m^2]
1	173	86.5	57.8	253
2	122	61	46.3	109
3	71	35.55	35.8	34.7
4	20	10	25	34.2

B. Control Structure

The control structure is depicted on Fig. 5. As it can be seen, the inverse kinematics block takes as inputs the end-effector position E, θ_3 and θ_4 and outputs θ_1 and θ_2. The algorithm consists of computing position of joint 2 (O_2) starting from E (by knowing orientations and lengths of links 3 and 4) and selecting one of the two admissible configuration for link 1 and 2. This configuration is chosen in such a way that the retracted state of Fig. 2b can be achieved.

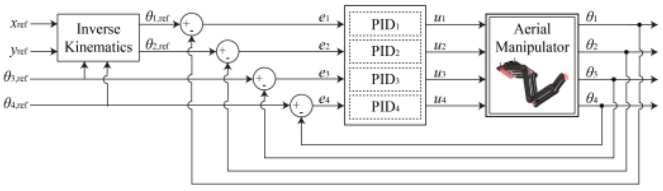

Fig. 5. PID-based structure for the position control of the aerial manipulator.

Afterwards, these joint coordinates feed four independent joint control loops, based on PID controllers with back-calculation as an anti-reset windup. This PID design is intended to compensate for the effective static friction torques, while reducing the resulting overshoots. Towards the controllers tuning, the same gains and clip values were set on each of the PIDs as follows:

$$\begin{aligned} \text{Proportional gain: } & K_p = 2.38 \\ \text{Integral gain: } & K_i = 0.00477 \\ \text{Derivative gain: } & K_d = 0.477 \\ \text{Lower clip value: } & C_- = -1 \\ \text{Upper clip value: } & C_+ = 1. \end{aligned}$$

These PIDs receive as reference signals the θ_i, in radians, for computing the command signals in terms of normalized motor voltages $-1 \leq u_i \leq 1$.

IV. PROTOTYPE DEVELOPMENT

A. Hardware

The proposed manipulator prototype, along with details displaying its mechanical properties are presented in Fig. 6. The proposed design stands on commercially available, widely used hardware components and aims at easing manufacture.

Specifically, the links consist of superimposed carbon fiber plates, drawing inspiration from the Radio Controlled (RC)

Model community. The tension into the belts was set using spiral springs tensioners (see Fig. 6b).

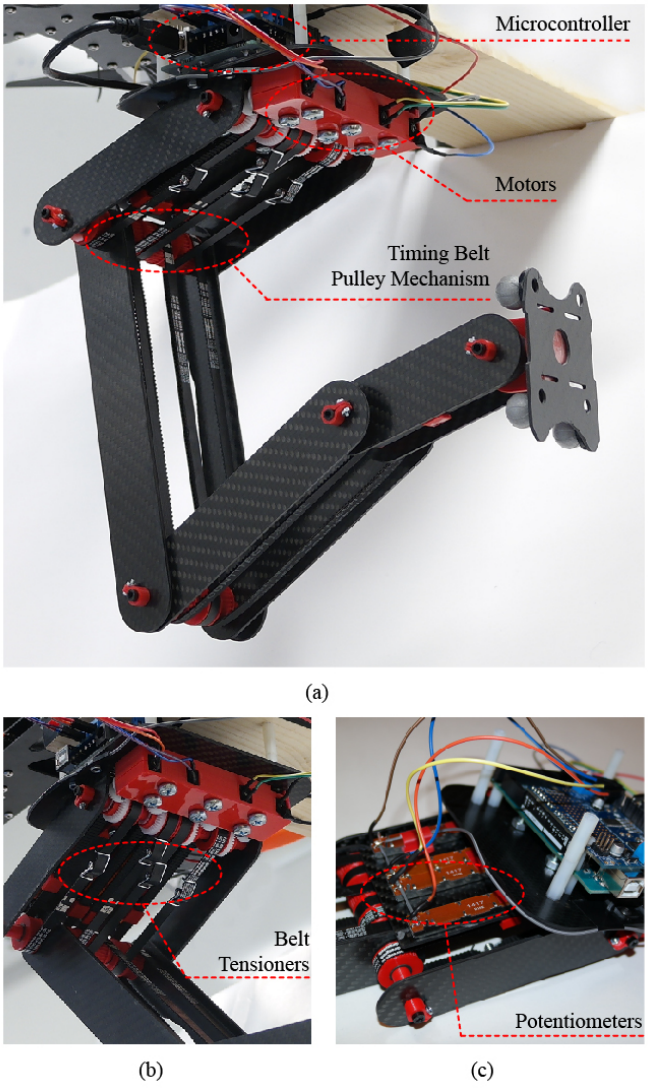

Fig. 6. Details of the components utilized for the development of the aerial manipulator: a) Front view portraying the motor-based motion mechanism, b) bottom view highlighting the tensioners used in the timing belts, and c) top view displaying the potentiometers used for displacement sensing along with the microcontroller board.

Bourns PTA4543-2015DPA103 linear slide potentiometers were used along with RS Components 6 mm width MXL rubber timing belts (Fig 6c), RS Components injection moulded acetal co-polymer bevel gears and Pololu 298:1 Micro Metal Gearmotor HP. The micro-controller board is an Arduino Mega 2560 endowed with an Adafruit Motor Shield V2.3 as a motor control board.

B. Software

The Arduino board stands as a low level joint controller with the ability to connect to a Robotic Operating System (ROS) [16] network. By being connected to a high level computer (such as the Intel NUC) via a USB serial communication and running the *rosserial_arduino* client library, it appears as a *node* over the network, therefore capable of *publishing* and *subscribing* to ROS messages. This software architecture improve versatility by enabling any platform running ROS to operate the manipulator.

V. EXPERIMENTAL EVALUATION

A. Workspace Exploration

The workspace was experimentally acquired by using a VICON motion capture system enabling sub-millimeter accuracy. The end-effector was endowed with a pod carrying markers as showed on Fig. 6. After discretizing every joint angle in 10° steps, all the possible combination were explored in a recursive manner. The result is given on Fig. 7.

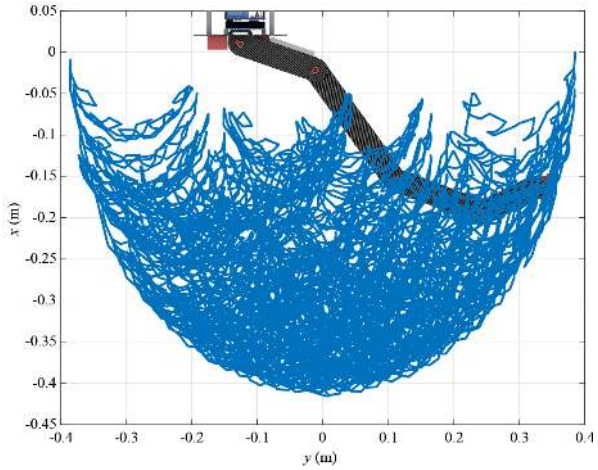

Fig. 7. Experimentally acquired workspace of CARMA.

B. Tracking Performance

The tracking capabilities of CARMA was demonstrated by performing a sinusoidal pick-and-place trajectory defined by:

$$x_{\text{ref}}(t) = 0.035cos(\pi/2cos(\pi t)+\pi)+0.3, \quad [\text{m}] \quad (2)$$

$$y_{\text{ref}}(t) = 0.12sin(\pi/2cos(\pi t)+\pi)+0.1, \quad [\text{m}] \quad (3)$$

$$\theta_{3,\text{ref}} = -\pi/4cos(\pi t), \quad [\text{rad}] \quad (4)$$

$$\theta_{4,\text{ref}} = -\pi/8cos(\pi t). \quad [\text{rad}]. \quad (5)$$

As previously, in Section V-A, the end-effector position has been acquired using a VICON motion capture system. The corresponding closed loop responses, along with their respective error values are provided in Fig. 8, while a comparison in the *xy*-plane of the reference trajectory, versus the real trajectory is given in Fig. 9. The resulting Root Mean Square Error (RMSE) values are 12.1 mm/9.6 mm along *x*/*y* axis, respectively, while the error was mainly due to uncompensated static frictions.

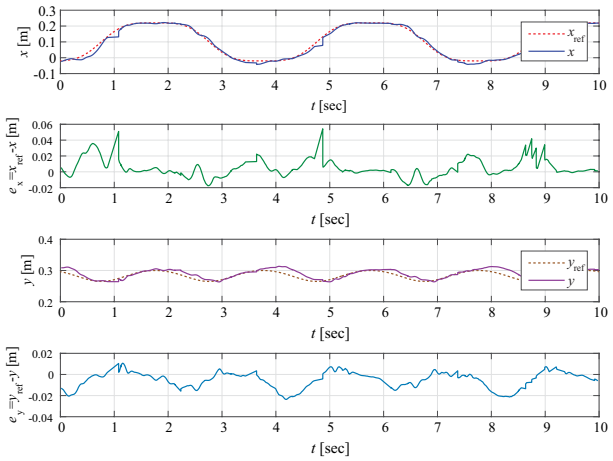

Fig. 8. Experimental closed loop responses for a planar trajectory defined by the x and y reference signals, along with their respective error values.

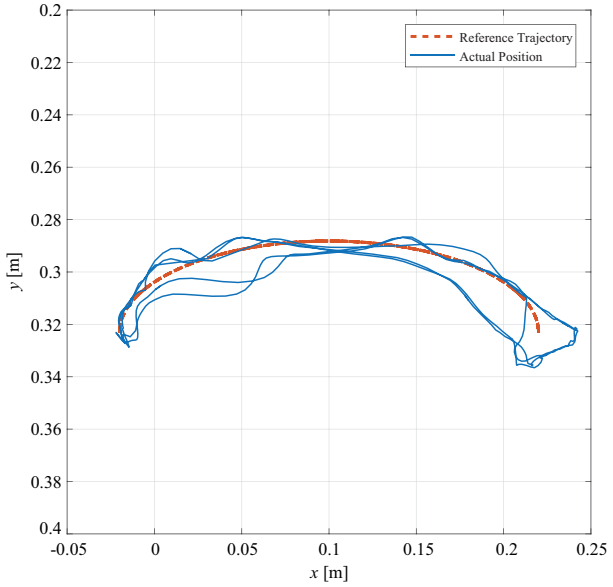

Fig. 9. Experimental closed loop response while tracking the resulting planar trajectory of Fig. 8.

C. Force/Torque Estimation

The inverse dynamic model given in Equation (1) for the forces and torques exerted on the base, due to free motions has been experimentally validated by setting up a dedicated test bench. Thus, an ATI Industrial Automation Nano17 6-DoF F/T sensor has been mounted between the base and the supporting structure. A human operator has been generating fast random oscillating reference signals through a game controller, which were feeding the inverse kinematics algorithm (see Fig. 10). Data from the F/T sensor and the potentiometers were collected and processed using MATLAB.

The proposed model was evaluated over the recorded joint positions and its output was compared with the F/T sensor data. Of course, the first and second order derivatives of the joint coordinate vector had to be estimated. This was done

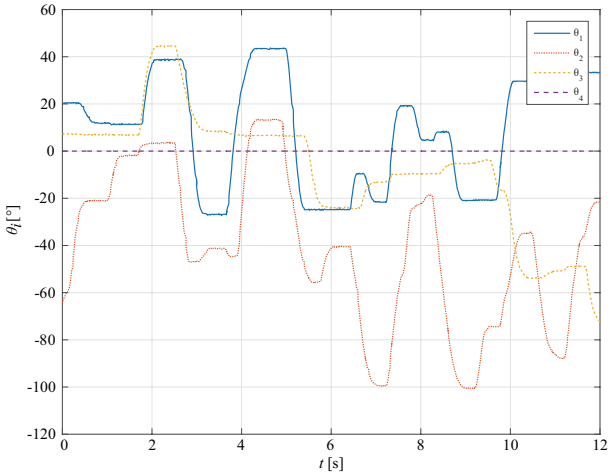

Fig. 10. Joint position signals acquired onto the test bench dedicated to F/T measurements

using the following second-order low-pass filter:

$$\ddot{x} + \frac{2}{\tau}\dot{x} + \frac{1}{\tau^2}x = \frac{1}{\tau^2}u, \tag{6}$$

with $\tau = 45$ ms being the time constant. It was discretized using the Zero-Order Hold (ZOH) method with a potentiometer based data sampling rate of $T_s = 12.1$ ms. In this case, the filtering action was used instead of smoothing for preserving causality, towards the development of a real-time applications.

Fig. 11 gives a comparison between simulation and experimental acquisition of F_x, F_y and M_z. As it can be seen, both signals are significantly noisy due to: a) first and second order derivatives amplifying noise on position signals, and b) the fast dynamics of the F/T sensor. A relative delay of $T_d = 83.2$ ms between measured and simulated data has been induced, mainly through filtering. For the sake of comparison, this delay was compensated in Fig. 11. The value of T_d has been experimentally determined by minimizing the fitting error.

The estimated F/T data appear to be valid, especially when the exerted wrenches reach a certain level (and therefore become of interest). The estimated F/T are very sensitive to static friction that may occur, while sliding the potentiometer pins. The unexplained peak at $t = 2$ s may result from such phenomenon, while the smoother characteristic of the simulated data can be explained by the required filtering. The lower values of measured M_z may result from the compliance of the belt and pulleys mechanism. Finally, it should be mentioned that there is indeed a dynamic relationship between the potentiometer positions and the joint angles, which was approximated as a static and affine one.

The present experiment validates the inverse dynamics algorithm as derived in Sec. III-A. Moreover, it demonstrates that the selected joint position sensors, consisting of linear potentiometers, are sufficiently accurate and precise for providing a relevant estimation of wrenches exerted on the base due to swift motions of the arm.

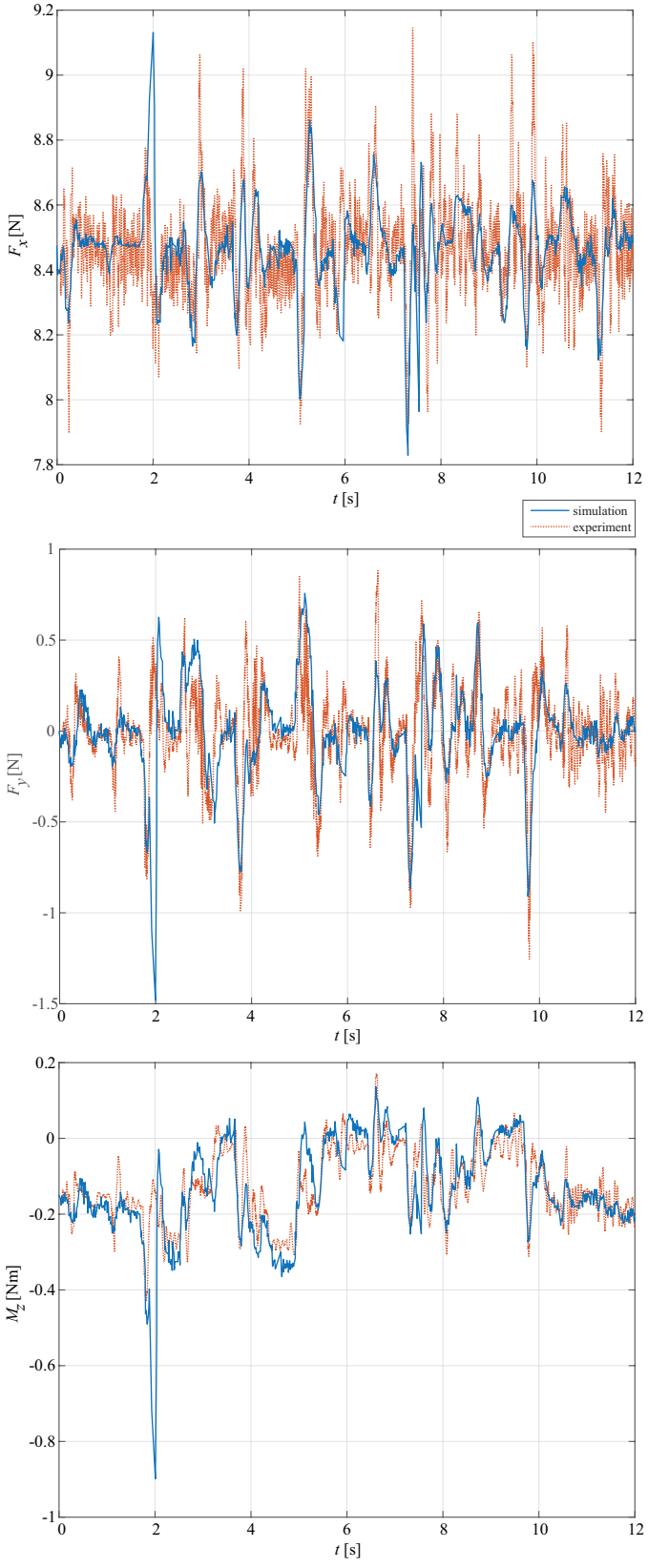

Fig. 11. Comparison plots between experimentally acquired and simulated vertical forces F_x, horizontal forces F_y and torques M_z exerted on the base.

VI. CONCLUSIONS

In this article, a novel aerial manipulator prototype has been presented, its dynamical model has been derived and a suitable control structure has been implemented. Furthermore, the manipulator's workspace was experimentally acquired, while its tracking capabilities were demonstrated over a pick-and-place trajectory and it was shown that the selected joint position sensors, in combination with the derived inverse dynamic model can provide, with reasonable delays, a relevant estimation of the wrenches exerted at the base toward real-time implementations.

Future work comprise the generation and implementation of a coupled control scheme for stabilizing the whole manipulator-UAV system by relying on the proposed model, as well as embedding the presented aerial manipulator for flight tests.

REFERENCES

[1] E. Fresk and G. Nikolakopoulos, "Full quaternion based attitude control for a quadrotor," in *European Control Conference*, July 2013.

[2] G. Nikolakopoulos, L. Dritsas, and S. Delshad, "Combined networked switching output feedback control with-region stability for performance improvement," *International Journal of Control*, vol. 87.

[3] AEROWORKS: Collaborative Aerial Workers - Horizon 2020 Project. [Online]. Available: http://www.aeroworks2020.eu/

[4] Q. Lindsey, D. Mellinger, and V. Kumar, "Construction of cubic structures with quadrotor teams," *Proc. Robotics: Science & Systems VII*, 2011.

[5] S. Shimahara, R. Ladig, L. Suphachart, S. Hirai, and K. Shimonomura, "Aerial manipulation for the workspace above the airframe," in *IEEE/RSJ International Conference on Intelligent Robots and Systems (IROS)*. IEEE, 2015, pp. 1453–1458.

[6] P. E. Pounds, D. R. Bersak, and A. M. Dollar, "Grasping from the air: Hovering capture and load stability," in *IEEE International Conference on Robotics and Automation (ICRA)*. IEEE, 2011, pp. 2491–2498.

[7] N. Michael, J. Fink, and V. Kumar, "Cooperative manipulation and transportation with aerial robots," *Autonomous Robots*, vol. 30, no. 1, pp. 73–86, 2011.

[8] Ascending Technologies GmbH. [Online]. Available: http://www.asctec.de/

[9] M. Orsag, C. Korpela, S. Bogdan, and P. Oh, "Valve turning using a dual-arm aerial manipulator," in *International Conference on Unmanned Aircraft Systems (ICUAS)*. IEEE, 2014, pp. 836–841.

[10] M. Fumagalli, R. Naldi, A. Macchelli, F. Forte, A. Q. Keemink, S. Stramigioli, R. Carloni, and L. Marconi, "Developing an aerial manipulator prototype: Physical interaction with the environment," *Robotics & Automation Magazine, IEEE*, vol. 21, no. 3, pp. 41–50, 2014.

[11] L. R. Buonocore, J. Cacace, and V. Lippiello, "Hybrid visual servoing for aerial grasping with hierarchical task-priority control," in *23th Mediterranean Conference on Control and Automation (MED)*. IEEE, 2015, pp. 617–623.

[12] C. D. Bellicoso, L. R. Buonocore, V. Lippiello, and B. Siciliano, "Design, modeling and control of a 5-dof light-weight robot arm for aerial manipulation," in *23th Mediterranean Conference on Control and Automation (MED)*. IEEE, 2015, pp. 853–858.

[13] K. Kondak, F. Huber, M. Schwarzbach, M. Laiacker, D. Sommer, M. Bejar, and A. Ollero, "Aerial manipulation robot composed of an autonomous helicopter and a 7 degrees of freedom industrial manipulator," in *IEEE International Conference on Robotics and Automation (ICRA)*. IEEE, 2014, pp. 2107–2112.

[14] B. Siciliano, L. Sciavicco, L. Villani, and G. Oriolo, *Robotics: Modelling, Planning and Control*. Springer, 2009.

[15] B. Siciliano and O. Khatib, *Springer Handbook of Robotics*. Springer, 2009.

[16] Robot Operating System (ROS). [Online]. Available: http://www.ros.org/